Electrochemistry of Ferrocene-Functionalized Phosphonium Ionic Liquids

ARTICLE *in* THE JOURNAL OF PHYSICAL CHEMISTRY C · OCTOBER 2011

Impact Factor: 4.77 · DOI: 10.1021/jp206927w

6 AUTHORS, INCLUDING:

Daniel Breadner
The University of Western Ontario
11 PUBLICATIONS **62** CITATIONS

SEE PROFILE

THE JOURNAL OF PHYSICAL CHEMISTRY C

ARTICLE

pubs.acs.org/JPCC

Electrochemistry of Ferrocene-Functionalized Phosphonium Ionic Liquids

Joshua E. F. Weaver,[†,§] Daniel Breadner,[‡] Fanguo Deng,[‡] Bala Ramjee,[†,∥] Paul J. Ragogna,[‡] and Royce W. Murray*[,†]

[†]Kenan Laboratories of Chemistry, University of North Carolina, Chapel Hill, North Carolina 27599, United States

[‡]Department of Chemistry, The University of Western Ontario, London, Ontario, N6A 3K7, Canada

Supporting Information

ABSTRACT: The synthesis of and voltammetry in undiluted form of several ferrocene-functionalized phosphonium ionic liquids is reported. Electron transport in the mixed valent diffusion layer around an electrode occurs primarily by $Fc^{+/0}$ electron self-exchange reactions, as opposed to physical diffusion of the ferrocenated phosphonium species. The apparent diffusion coefficients for electron transport and for the counterions of the ionic liquid, and in particular their activation energy barriers, are similar to one another, evidence for the control of rates of electron transport by relaxation of the counterion atmosphere. For a net transport of electronic charge to accompany electron transfer, counterion displacement must occur to relax the charge displacement associated with the electron transfer. The ferrocenated phosphonium ionic liquids thus behave in a manner like that of previously investigated redox ionic liquids based on combinations of redox groupings with imidazolium and with short-chain polyether functionalities.

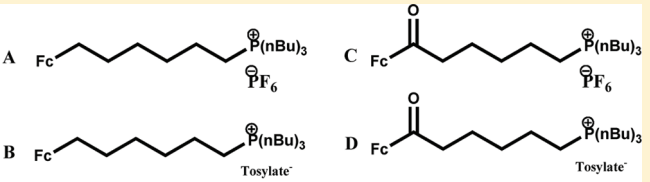

Electrochemistry in Ferrocene-functionalized Phosphonium Ionic Liquids

INTRODUCTION

In recent years ionic liquids have begun to move from the realm of novel chemical materials to materials with many practical applications. These uses are centered on the unique property of being both innately conducting and liquid and are often associated with electrochemical applications.[1] Practical applications now include use as electrolyte−solvents in batteries, fuel cells, and capacitors. Some recent studies have examined the behavior of various solutes in ionic liquids,[2] molecular force fields of ionic liquids,[3] hydrogen oxidation in ionic liquids at a platinum electrode surface,[4] density estimation of ionic liquids,[5] the applicability of Marcus theory to ionic liquid redox processes,[6] and the evaluation of new materials such as tetraalkylphosphonium polyoxometalate ionic liquids.[7]

This group has investigated the electrochemical properties of various classes of ionic liquid materials that have included redox active polyether hybrids, DNA complexes, and imidazolium systems.[8−17] Redox functionalized ionic liquids inherently offer unique opportunities for investigations of electron transfer and mass transport in melt phases, when used in their undiluted forms where electron hopping dominates. These materials often have melting points below 100 °C and are sufficiently ionically conductive as to permit quantitative voltammetry in the undiluted state. They can be designed to incorporate a variety of redox species, either appended to or as a counterion[8] of a molecular ionic liquid. The present study is of the redox active ferrocenated phosphonium ionic liquids shown in Figure 1, describing their synthesis and electron transport properties.

Our previous studies have focused on investigating and understanding the rates of mass and electron transport in semisolid media, choosing as model media, redox functionalized ionic liquids. With very high redox site concentrations, such as ferrocene in the 1−2 M range, the neat melt materials are concurrently both electron and ionically conductive. An important property of the undiluted redox ionic liquids is that the spacing between redox sites is small, allowing facile electron self-exchange (hopping). The viscosities of the neat materials are substantial, so that physical diffusion of redox sites is greatly retarded, and except for redox couples with nominally very slow electron transfers,[12] becomes slower than the transport of electrochemical charge by electron hopping. The electron hopping process is initiated by electrochemical voltammetry, which generates a mixed valent layer at the electrode interface.

As originally pointed out by Buttry and Anson,[18] the general expression for the combined electron hopping and physical diffusion processes, that is, the apparent diffusion (D_{APP}), is the transport summation of the Dahms−Ruff equation:[19,20]

$$D_{APP} = D_{PHYS} + D_{E,TRANS} = D_{PHYS} + \frac{k_{EX,APP}\delta^2 C}{6} \quad (1)$$

Received: July 20, 2011
Revised: August 23, 2011
Published: September 09, 2011

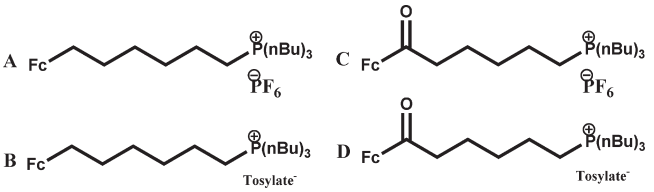

Figure 1. Four phosphonium ionic liquids include two examples of alkyl chain (A and B) and acyl chain (C and D) linkers between the ferrocene and the phosphonium group, each with either a hexafluorophosphate or tosylate counterion. The ionic conductivity of the melt D with a tosylate counterion proved to be very small, generating iR_{UNC} effects too severe to obtain satisfactory charge transport data in the pure melt.

where D_{PHYS} is the actual physical diffusion coefficient of the redox sites, and $D_{E,TRANS}$ is the electron diffusion coefficient that describes the rates of electron transport. By the right-hand term, $D_{E,TRANS}$ can be translated[20] into $k_{EX,APP}$, an *apparent* electron self-exchange rate constant. The translation is based on an assumed hexagonal packing model in which δ is the equilibrium center-to-center distance between redox sites, C is the bulk concentration of redox sites, and 6 accounts for directional electron hopping possibilities. The values of D_{PHYS} in previous undiluted redox ionic liquid been shown to normally be much smaller than those of D_E. The general range of parameters in the phosphonium ionic liquids is similar, and we presume here that $D_{PHYS} \ll D_{E,TRANS}$ in them, that is, $D_{E,TRANS} = D_{APP}$.

It is important to understand that $D_{E,TRANS}$ describes the rate of electron *transport*, not the rate of electron *transfer*. The current study makes use of an ion association model by Marcus[21] and the related ion atmosphere relaxation model.[9,10,17] The ion atmosphere relaxation model proposes that when an electron hops between oxidized and reduced species, as part of the diffusive charge transport process, the rate-determining step for charge transport is the rearrangement of the counterion to relax the Coulombic dis-equilibrium caused by the electron displacement. The intrinsic rate of electron transfer thus can be faster than that of electron transport. Related ideas apply to proton transfers.[22] The ion atmosphere relaxation model has been demonstrated to account for electron transport rates in redox ionic liquids by comparisons[9,10,14] of an observed redox species' diffusion rate (D_{APP}) to measurements of the diffusivity (D_{CION}) of the melt counterions and comparisons of the associated activation energy barriers. The equality of these parameters, that is, $D_{APP} = D_{CION}$ and $E_{ET} = E_{CION}$, signals control of electron transport by the rate of ion atmosphere relaxation.

The phosphonium materials studied here add to an already developing understanding of electron transfer and mass transport in semisolid phases. Phosphonium ionic liquids present new and interesting challenges for electrochemistry in the solid state because of their reported ability to pack and even form liquid crystalline phases.[23] Although this report will not delve into these materials' liquid crystalline natures, it does show that these materials have some structure-related differences in their diffusivity in the melt phase, based on the electrochemical studies. The study concludes that, as in previous redox ionic liquids,[9,10,17] electron transport is limited by the rate of counterion relaxation.

EXPERIMENTAL SECTION

Chemicals and Reagents. All phosphonium ionic liquid samples were synthesized and furnished by the Ragogna Laboratory at the University of Western Ontario. Solvents and reagents were used with no further purification unless otherwise noted.

Synthesis. Synthetic manipulations were performed either in an M Braun Labmaster 130 N_2-filled drybox or with standard Schlenk line techniques, unless otherwise indicated. Flash column chromatography was with 70−230 mesh ASTM silica gel 60, and thin layer chromatography (TLC) was on silica gel 60 F_{254} TLC plates. TLC and flash column chromatography were done using varying ratio mixtures of hexanes and acetone as indicated in specific procedures. Solution NMR data were collected on a Varian Mercury 400 MHz using $CDCl_3$ as a solvent. The ^{31}P NMR spectra were referenced to 85% phosphoric acid at 0 ppm. Electrospray ionization mass spectrometry (ESI-MS) data were collected on a Micromass LCT mass spectrometer. Thermogravimetric analysis (TGA) was conducted using a Mettler Toledo TGA 851 instrument, heating a 5−10 mg sample at 10 °C/min from 25 to 600 °C. Ferrocene purchased from Aldrich Chemical Co. was twice sublimed and stored in the drybox. Oxalyl chloride, 3-bromopropanoic acid, 6-bromohexanoic acid, mercury chloride, zinc granules, aluminum trichloridem, and all other chemicals were purchased from Aldrich Chemical Co. and used as received. Common organic solvents from Caledon Laboratories were dried using the Innovative Technology Inc. Controlled Atmospheres Solvent Purification System, which utilizes dual-alumina columns. All dry solvents were stored in Strauss flasks over N_2 or in the drybox over 4 Å molecular sieves. *n*-Butyl phosphine donated by Cytec Technology Corp. was used as received.

Synthesis of Fc−CO(CH$_2$)$_5$Br. At room temperature, a double-necked round-bottom flask was charged with 6-bromohexanoic acid (21.0 mmol) in toluene (30 mL) with stirring under N_2; 1.2 equiv (3.17 g, 25.2 mmol) of oxalyl chloride were added dropwise, followed by addition of 0.3 mL of dimethylformamide (DMF). Continuing stirring for 30 min and then for a further 90 min at 55 °C, the reaction mixture was cooled to room temperature (r.t.) and the toluene removed in vacuo. Aluminum trichloride (1.2 equiv., 3.22 g, 24.2 mmol) dissolved in 80 mL of dry CH_2Cl_2 in the drybox was transferred to the Schlenk line and then added to the 6-bromohexyl chloride under N_2. The resulting solution was added dropwise to 40 mL of a stirred, dry CH_2Cl_2 solution of ferrocene (3.91 g, 21.0 mmol, loaded in drybox) in a separate 250 mL round-bottom flask. The reaction mixture was allowed to warm to r.t. over 3 h and washed with water (2 × 10 mL). The organic layer was separated, dried with $MgSO_4$, and the solvent evaporated. The product was purified by passing through a silica gel column in a 2.5% acetone in hexane solution (4.36 g, 57%). ^1H NMR ($CDCl_3$, δ/ppm): 1.51 (m, 2H), 1.71 (q, 2H), 1.90 (q, 2H), 2.70 (t, 2H), 3.42 (t, 2H), 4.17 (s, 5H), 4.47 (t, 2H), 4.75 (t, 2H); ^{13}C NMR ($CDCl_3$, δ/ppm): 23.8, 28.3, 32.9, 24.0, 39.6, 69.5, 70.0, 72.4, 79.3; ESI MS $[M^+]$ = 362, $[M^+-HBr]$ = 282, $[M^+-C_5H_{10}Br]$ = 213, $[M^+-(CO)C_5H_{10}Br]$ = 185.

Synthesis of Fc−(CH$_2$)$_6$Br. The reduction of Fc−CO(CH$_2$)$_5$Br followed that by Vogel et al.[24] in the reduction of acylated ferrocene. Fresh Zn/Hg amalgam (prepared by 5 min stirring 2.5 g of Zn granules and 0.169 g of $HgCl_2$ in 3 mL of water plus 0.2 mL of conc. HCl, then discarding the aqueous supernatant) was added to a mixture of 6 mL of water and 8 mL of conc. HCl in a 250 mL double-necked round-bottom flask. To this was promptly added, dropwise over 5 min, a solution of 10 mL of acylated ferrocene (Fc−CO(CH$_2$)$_5$Br) (0.908 g, 2.51 mmol). The reaction mixture was set to reflux for 18 h. Two 2 mL portions of conc. HCl were added to the mixture after 1 and 3 h,

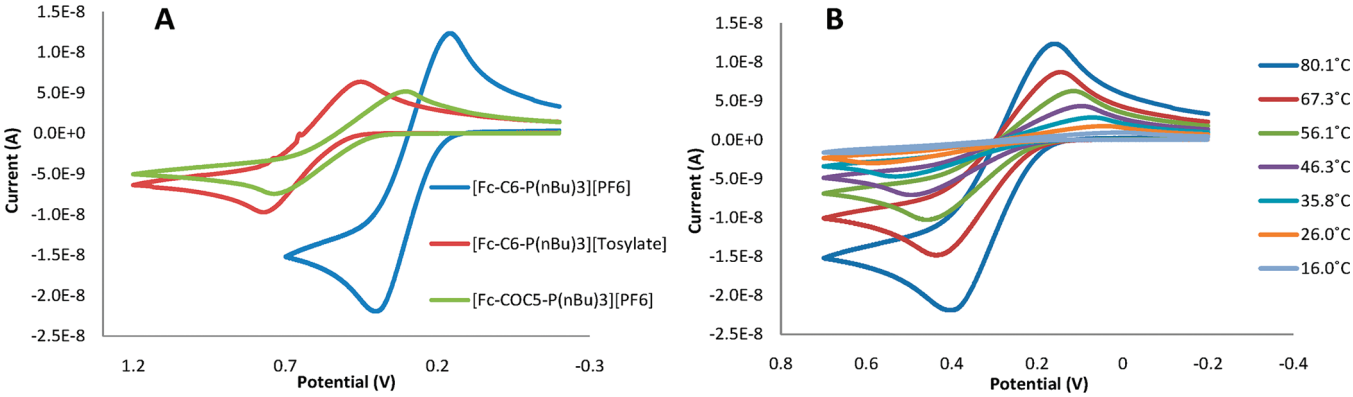

Figure 2. Panel A: Cyclic voltammetry showing differences in E_0' between alkyl and acyl linkage to ferrocene phosphonium ionic liquid (compare blue and green CVs), in neat melt at 80 °C, and the effect of counterion on both the E_0' and the ionic resistance of the pure melt (compare blue and red CVs). Panel B: Temperature has a substantial effect on melt ionic resistance and uncompensated *iR* drop, as seen by large peak splittings for the alkyl linked IL A.

respectively. The resulting mixture was allowed to cool to r.t., 10 mL toluene added, and the organic layer separated. Removing the volatiles in vacuo, the resulting product was purified using a silica gel column and a 1.25% acetone in hexanes solution (0.637 g, 73%). ^{1}H NMR ($CDCl_3$, δ/ppm): 1.35 (m, 2H), 1.46 (m, 2H), 1.52 (m, 2H), 1.86 (q, 2H), 2.33 (t, 2H), 3.41 (t, 2H), 4.05 (s, 4H), 4.10 (t, 5H); ^{13}C NMR ($CDCl_3$, δ/ppm): 27.9, 28.6, 29.4, 30.9, 33.9, 66.8, 67.1, 67.8, 68.1, 68.2, 68.5, 89.1; ESI MS [M^+] = 348, [M^+−HBr] = 268, [M^+−$C_5H_{10}Br$] = 199.

General Procedure for the Preparation of Ferrocene-Containing Ionic Liquids. The bromide salts of the alkylated or acylated ferrocenes were prepared by reaction in DMF solutions by the following general procedure. To 5 mL of a DMF solution of the ferrocene in a 100 mL round-bottom multinecked flask was added, dropwise with stirring, 10 mL of a DMF solution of tributyl phosphine. A reflux condenser was attached and the solution heated to 70 °C under N_2. The progress of the reaction was monitored by ^{31}P NMR until no further spectral change was observed. The volatiles were removed in vacuo at 100 °C. The detailed specific procedures for each ionic liquid salt are given in the Supporting Information.

The PF_6^- and tosylate salts of the ionic liquids were prepared by ion metathesis with $NaPF_6$ and toluene sulfonic acid, respectively.

Shorthand notations used in figures for the four ferrocenated phosphonium ionic liquids (Figure 1) are: A [Fc−C_6−$P(Bu)_3$]-[PF_6], B [Fc−C_6−$P(Bu)_3$][tosylate], C [Fc−COC_5−$P(Bu)_3$]-[PF_6], and D [Fc−COC_5−$P(Bu)_3$][tosylate].

Dilute Solution Voltammetry. The general solution behavior was checked by cyclic voltammetry (CV, typical v = 50, 100, and 200 mV/s) on ca. 1.0 mM CH_2Cl_2 or CH_3CN solutions of the phosphonium ionic liquids containing 0.1 M Bu_4NClO_4 supporting electrolyte. The electrodes were 1.6 mm diameter Pt disk working, Pt mesh counter, and aqueous Ag/AgCl/0.1 M NaCl reference and were controlled by a CHI Instruments Electrochemical Workstation.

Electrochemistry of Undiluted Ionic Liquids. The electrochemistry of the pure ionic liquids was carried out as described previously for redox polyether hybrids.[9,14] Approximately 15−20 mg of the ionic liquid is drop-cast from CH_2Cl_2 solution onto a small platform in which are exposed four electrode wire tips—a 25 μm diameter Pt disk working electrode, Ag wire quasi-reference, and two 0.4 mm diameter Pt disk electrodes. AC potential bias was applied between the two 0.4 mm Pt disks for AC impedance spectroscopy measurements (of ionic conductivity). One of the 0.4 mm Pt disks was used as a counter electrode in voltammetry on the Pt microdisk. The wire tip platform is formed in a 0.25" stainless steel tube by casting with an epoxy resin. Drop-cast films of the ionic liquid are dried at ca. 75 °C for ≥12 h by mounting the electrode assembly in a temperature-controlled, evacuated chamber,[25] to ensure complete dryness; the residual solvent plasticizes ionic liquids and alters transport parameters.

Voltammetry and AC impedance measurements were performed in a Faraday cage using a CH Instruments Electrochemical Workstation, with the cell assembly under vacuum. To assess activation parameters, measurements were taken over a range of temperatures with care to ensure thermal equilibration.

AC impedance measurements of the melts were taken at from 1 Hz to 100 kHz with a 0 V DC bias, 2 s of quiet time, and 5−400 mV amplitude. The larger amplitudes were needed when the melt conductivity was very low. Ionic conductivities were calculated from the real x-axis intercept of a Nyquist plot. CV was performed with a 30 s quiet time and 10 mV/s scan rate. Potential steps for chronoamperometry were judged from the ferrocene redox potentials and the extent of ohmic drop as judged from a preliminary CV at each temperature. Current−time responses were assessed over 400 s, with a 450−600 s quiet time. Transport was sufficiently slow that diffusion was always linear.

RESULTS AND DISCUSSION

Dilute Solution and Undiluted Melt Voltammetry. Cyclic voltammetry (CV) of the ferrocenated phosphoniums in dilute solutions and as undiluted (neat) melts was conducted to inspect for electrochemical purity and to evaluate their formal potentials ($E^{o\prime}$). $E^{o\prime}$ in dilute CH_3CN solution for A (Figure 1) is 445 mV versus Ag/AgCl, while that for C, 732 mV versus Ag/AgCl, is shifted to more positive potential owing to the carbonyl group's substituent effect (Figure S-2A of the Supporting Information). The solution voltammetry was also compared to that of model ferrocenes, ethylferrocene and acetylferrocene; they show no distinct $E^{o\prime}$ differences from phosphonium ionic liquid molecules in dilute solutions (Figure S-2B of the Supporting Information).

The voltammetry of the pure melts was inspected to ensure that the materials had not been electrochemically degraded by the drop-casting and drying procedure. No extraneous waves were seen.

Table 1. Collected Transport Data for Ferrocene Phosphonium Ion Liquids[a]

sample, C_{Fc}, mol/cm^3	T (K)	D_{APP} (cm^2/s) ($\times 10^{-9}$)	$D_{APP,CORR}$ (cm^2/s) ($\times 10^{-9}$)	$k_{EX,APP}$ (M^{-1} s^{-1}) ($\times 10^5$)	$k_{EX,CORR}$ (M^{-1} s^{-1}) ($\times 10^5$)	$E_{A,ET}$ (KJ/mol)	$E_{A,ET,CORR}$ (KJ/mol)	σ_{ION} (S/cm) ($\times 10^{-6}$)	D_{CION} (cm^2/s) ($\times 10^{-10}$)	$E_{A,ION}$ (KJ/mol)
$[Fc-C_6-P(nBu)_3]^+$ $[PF_6]^-$	353	15.3	12	52.3	41.7	48	47	13	21.5	47
2.0×10^{-3}	340	8.3	6.4	28.4	21.9			7.4	11.4	
	329	5.1	3.9	17.4	13.5			4.5	6.7	
	319	2.8	2.2	9.5	7.6			2.7	3.9	
	309	1.5	1.2	5.1	4.0			1.5	2.1	
$[Fc-C_6-P(nBu)_3]^+$ [tosylate]$^-$	350	3.5	3.0	21.7	13.4	65	52	5.3	8.3	40
2.0×10^{-3}	339	2.4	2.0	13.5	7.7			3.5	5.3	
	329	1.2	1.0	4.0	3.5			2.3	3.4	
	319	0.7	0.64	2.5	2.2			1.5	2.2	
	309	0.4	0.33	1.2	1.1			0.98	1.4	
$[Fc-COC_5-P(nBu)_3]^+$ $[PF_6]^-$	350	6.4	3.9	25.9	16.0	55	53	1.5	4.1	65
2.0×10^{-3}	339	4.0	2.3	16.1	9.3			0.81	2.1	
	329	2.7	1.4	11.0	5.9			0.38	1.0	
	319	1.3	0.69	5.2	2.8			0.19	0.5	
	309	0.5	0.28	2.0	1.2			0.09	0.2	
*$[Fc-C_6-Im-Bu][PF_6]$	298	10.0	1.2	32.0	37	56	58		1.7	58
2.5×10^{-3}										

[a] Note the similarities of the (corrected) electron and ion transport activation energies. For comparison, a data sample from a recent study (ref 14) of a ferrocenated imidazolium ionic liquid is included at the bottom.

CV) of three of the four ferrocenated phosphonium ionic liquids is shown in Figure 2. Immediately evident is the very modest levels of ionic conductivity of these materials. Even at elevated temperatures (80 °C) and with use of a 25 μm diameter Pt microelectrode, all of the CVs exhibit substantial peak potential separations (ΔE_{PEAK}), reflecting large iR_{UNC}. CVs at room temperature are quite distorted (Figure 2B). Also seen in Figure 2 is the substantial influence of the counterion on ionic conductivity. The melts with tosylate counterion were less conductive (larger ΔE_{PEAK}); the ionic liquid D was so poorly conductive (and viscous) that reliable transport data could not be obtained, even at elevated temperatures. Overall, the phosphonium ionic liquids are somewhat less ionically conductive than are polyether-based ionic liquids.[8b,12,15]

The counterion also plays a strong role in the ferrocene apparent formal potential in the melts, as illustrated in Figure 2A by the quite different $E^{o\prime}$ for the isostructural A and B with PF_6^- and tosylate counterions, respectively. Due to the necessary use of a silver quasi-reference in the melt electrochemistry setup, a counterion effect on the reference electrode potential could possibly play a role in the above shift in apparent $E^{o\prime}$, although ion association effects are also likely. Due to the reference electrode issue, we make no comparisons between the melt $E^{o\prime}$ and dilute solution values. It is worth noting that the reference electrode uncertainty has no consequence on the chronoamperometric experiments, since the potential step sizes are judged from concurrent CVs taken in the melt.

Figure 2B shows the temperature dependence of CV peak currents and ΔE_{PEAK} values; peak currents are substantially diminished and ΔE_{PEAK} values substantially enhanced at room temperature relative to 80 °C. The fluidity of the melts is also markedly lower at room temperature. The substantial temperature effects on currents and ΔE_{PEAK} signal large activation barriers for both electron transport and ion transport; in fact we will see below that not only are both barrier energies large, they are close to being the same.

Electron Transport. As in previous experiments[8−17] on other redox ionic liquids, potential step chronoamperometry is used to measure the dynamics of charge transport—that is, the apparent electron diffusion coefficient ($D_{E,TRANS}$) in the ferrocenated phosphonium ionic liquids. The potential step for each temperature in each melt and, judged from a concurrently taken CV, is calculated to overwhelm ΔE_{PEAK} effects (e.g., Figure 2) and so is well beyond the CV peak current potential. The current versus time$^{-1/2}$ Cottrell plots[25] (Figure S-3 of the Supporting Information) obtained from the current−time transients are linear with zero intercept origins. Owing to the slow charge transfer diffusion rates, linear diffusion is maintained. Values of D_{APP} obtained from Cottrell plot slopes are presented in Table 1. As noted earlier, based on ample previous experience,[9−16] and the steric bulk of the phosphonium cation, its physical diffusion rate is assumed to be sufficiently slow that D_{PHYS} is neglected in eq 1. That is, electron hopping ($D_{E,TRANS}$) is the primary source of charge diffusion and is equated with D_{APP}. This assumption has been amply justified by actual experimental measurements of D_{PHYS} for other redox ionic liquid species selected for very slow electron transfer dynamics so as to force physical diffusion control.[12]

The electron transport data (D_{APP} = $D_{E,TRANS}$) can be expressed in terms of apparent rates of electron self-exchange $k_{EX,APP}$ by use of the right-hand side of eq 1, where the rate of electron hopping is modeled by a cubic lattice so as to account for redox site concentration and the center to center site spacing (i.e., the distance of an electron hop). The $k_{EX,APP}$ results for the three ferrocenated phosphonium salts for which measurements were possible are given in Table 1. Also given, for comparison, are some recent data[14] for a ferrocenated imidazolium ionic liquid.

The temperature dependency of $k_{EX,APP}$ can be inspected with plots of $\ln[k_{EX,APP}]$ against reciprocal temperature (Arrhenius plot, eq 2). These plots are linear (Figure 3, red points) with slopes reflecting (Table 1, Figure 3) the heats of activation for the

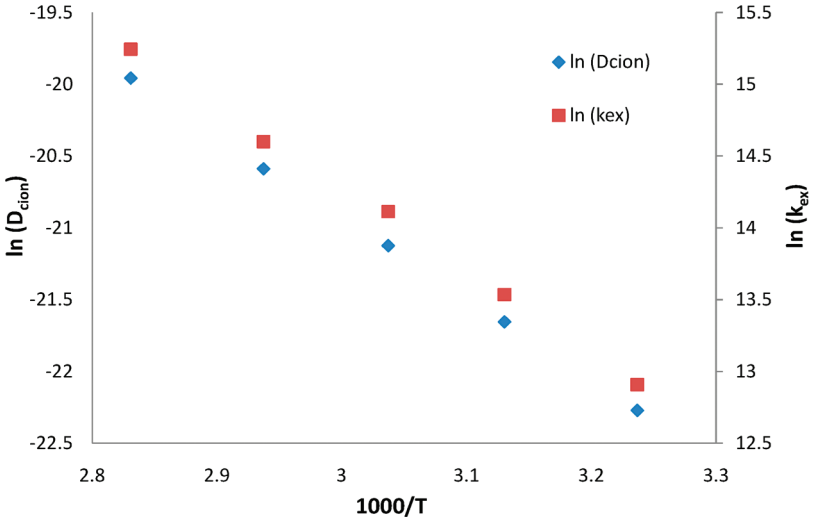

Figure 3. Nearly identical slopes that are found in the $k_{EX,CORR}$ and D_{CION} Arrhenius plots for phosphonium ionic liquid A are indicative of ion-atmosphere relaxation dominated electron transport.

electron transport process.

$$\ln[k_{EX,APP}] = -[E_{A,ET}/RT] + \ln[A] \quad (2)$$

where R is the ideal gas constant and A the pre-exponential factor of the Arrhenius equation. Because the electron self-exchange reaction is symmetrical, its entropy of activation is zero,[26] so the activation barrier heat energies are also free energies of activation.

Electronic migration effects occur in redox melts when electron diffusion coefficients (i.e., $D_{E,TRANS}$) are comparable to or larger than the diffusion coefficients of the counterions (evaluated below, D_{CION}). Such a mismatch of electron and counterion mobility can produce a local electrical field gradient that accelerates the rate of electron hopping, inflating the observed D_{APP} values, as pointed out by Saveant and Andrieux.[27] We have shown in previous work[12] that the bias caused by an electronic migration effect can be corrected based on the published theory[27] (details amplified in Supporting Information and Table S-1). Applying this correction to the D_{APP} data in Table 1 produces $D_{APP,CORR}$ values that are converted using eq 1 to corrected apparent electron transfer rate constants $k_{EX,APP,CORR}$. Corrected activation parameters ($E_{A,ET,CORR}$) were obtained with revised activation plots. These migration-corrected data are given in Table 1. As seen, the electronic migration correction is a modest factor.

Counterion Transport Rates. Testing the ion atmosphere relaxation model that has been successfully applied to other ionic liquid systems[9,10,14,16] requires measurement of the physical diffusivity of the melt counterions. The counterion diffusion coefficient (D_{CION}) can be calculated from ionic conductivity data (Table 1) using the Nernst−Einstein equation

$$\sigma_{ion} = \frac{F^2}{RT}[z_{Fc}{}^2 D_{Fc} C_{Fc} + z^2_{counterion} D_{counterion} C_{counterion}] \quad (3)$$

where z, D, and C are the charge, diffusion coefficient, and concentration of the noted species, respectively, F is Faraday's constant, and σ_{ion} is the measured ionic conductivity of the undiluted ionic liquid.[12] The ionic conductivities (σ_{ion}) were measured using AC impedance (Figure S-4 of the Supporting Information) using an electrode specific cell constant. Making the reasonable assumption that the physical diffusivity of the bulky phosphonium cation (D_{PHYS}) is small in comparison to that of the PF_6^- and tosylate counterions, diffusion coefficients D_{CION} of the latter can be calculated from eq 3. These data and the corresponding activation barriers $E_{A,ION}$ for counterion diffusion taken from Arrhenius plots are given in Table 1.

Our ion atmosphere relaxation interpretation[9,10,14,16] of electron transport control in mixed valent redox-labeled ionic liquids grew out of previous investigations in melts of redox species having appended short polyether chains. These PEG-labeled materials included melts of diverse redox species—Co and Ru bipyridine and phenanthroline complexes, ferrocene and cobalticenium derivatives, and Au_{25} nanoparticles—in a variety of states including pure melts and melts plasticized by CO_2 sorption.[8−16] Given the diversity of the redox couples, we initially expected[12] that the electrochemical transport measurement, through eq 1, would give convenient access to electron dynamics behavior in semisolid media (the highly viscous redox melts). However, obtained D_E results seemed to be always about the same, regardless of the redox couple, and attention turned to control of the rate of electron transport by the rate of counterion transport. The formulation of the ion atmosphere relaxation model accommodated the entire range of electron transport results for polyether-based ionic liquid melts. Since then, we have examined other types of redox ionic liquids, notably a variety of ferrocene-labeled imidazolium ionic liquids[14] that also fit within the ion atmosphere relaxation body of data—the counterion transport rate governs electron transport.

The results from the present phosphonium ionic liquids behave as expected from the ion atmosphere relaxation model. Table 1 shows that values of $D_{APP,CORR}$ and D_{CION} are very similar. Log−log plots of $k_{EX,CORR}$ (which is proportional to $D_{APP,CORR}$ by eq 1) and counterion diffusion coefficients D_{CION} are shown in Figure 4A. While there is some scatter in the slopes of these plots, the average collective slope is 1.0, which means that $k_{EX,CORR}$ (and $D_{APP,CORR}$) vary linearly with D_{CION}. Figure 4B superimposes the new phosphonium data on a previously reported[10] aggregate plot of a number of redox polyether ionic liquids; the phosphonium data lie

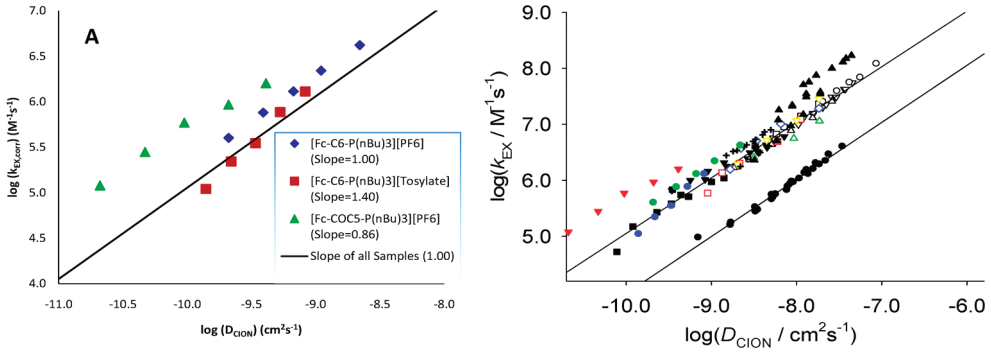

Figure 4. Panel A: Log−log plot for phosphonium data in Table 1. The solid line ("slope of all samples") has slope of 1.00 and is the line observed as a slope of 1.00 fit to all previous polyether melt data.[10] Panel B: Plot of all previous polyether melt data with data from panel A added; those points lie at lower left. The (edited) legend[10] for the previous data is: neat $[Cp_2Co](MePEG_{350}SO_3)$ and $MePEG_{350}$-plasticized $[Cp_2Co](MePEG_{350}SO_3)$ (▲), 1:1 mol/mol $[Cp_2Co](MePEG_{350}SO_3)/[FcTMA](MePEG_{350}SO_3)$ mixed melt (△) over a range of temperatures (25−70 °C), $[Co(phen)_3](MePEG_{350}SO_3)_2$ plasticized with $MePEG_{350}$ (♦), $[Co(phen)_3](MePEG_{350}SO_3)_2$ (●) and $[Co(bpy(CO_2MePEG_{350})_2)_3](ClO_4)_2$ (▼), both plasticized with liquid CO_2 (over a range of temperatures), $[Co(bpy(CO_2MePEG_{350})_2)_3](ClO_4)_2$ + xLiClO$_4$ (■) (x = 0−1.31), $[Ru(bpy(CH_2MePEG_{350})_2)_2](CN)_2$ plasticized with CO_2 (over a range of temperatures) (▲), and $[Ru(bpy(CO_2MePEG_{350})_2)_3][X]_2$, where X = ClO_4^- or a combination of ClO_4^- and I^- (●, points in line offset to the right). The slope of line shown is 1.0.

at lower right. The aggregate plot has a unity slope, and two of the three phosphonium data sets comfortably "disappear" into the large body of previous data. The data from C have a near-unity slope but are displaced above the main body of results. Two other previous data sets in Figure 4B are also displaced from the main body of data, while retaining a unity slope. The reason for such displacements is unclear.[10]

The electron transport and counterion diffusivity data collected in Table 1 are fully consistent with the ionic atmosphere relaxation model developed previously. It is nonetheless worthwhile to examine the possible sources of bias and error in the transport measurements. The presentation of data in Figure 4B is on a log scale, which tends to suppress the data "scatter"; on a linear scale variations of factors of ±3X in the diffusion numbers would be evident. These measurements are challenging, amounting to conducting voltammetry in a near-solid state with massive iR_{UNC} effects. The iR_{UNC} effects comprise a major source of data uncertainty. Another is that transport in ionic liquids is very sensitive to diffusion-plasticization by residual solvents. While the drying procedures employed are somewhat rigorous, the residual solvent remains a potential factor. Another factor is possible error in determining the ion conductivities. When ion conductivity is very low, our AC impedance equipment capability can be hard pressed; an example is the data scatter in Figure S-4 of the Supporting Information, where very low frequencies and elevated AC amplitudes had to be employed to extract the impedance spectrum. Finally, as pointed out by a reviewer, the molar volumes of the reduced and oxidized ferrocenated phosphonium species may change owing to the added counteranion (i.e., $(Fc-R-PBu_3^+X^- \rightarrow Fc-R-PBu_3^{+2}(X^-)_2)$, with possible associated perturbations of ionic liquid density and/or concentration in the transport layer that are not accounted for in evaluating $D_{APP,CORR}$ and D_{CION} values. Such effects are unlikely however to alter the relative values of, and correlation between, $D_{APP,CORR}$ and D_{CION}.

■ ASSOCIATED CONTENT

Ⓢ Supporting Information. Synthetic details, further voltammetry, and electron migration correction. This material is available free of charge via the Internet at http://pubs.acs.org.

■ AUTHOR INFORMATION

Corresponding Author

*E-mail: rwm@unc.edu.

Present Addresses

[§]Ionic Liquids Laboratory, Department of Chemistry and Biomolecular Engineering, North Carolina State University, Raleigh, NC 27695, United States.

[‖]Department of Chemistry and Biochemistry, Old Dominium University, Norfolk, VA 23529, United States.

■ ACKNOWLEDGMENT

This research was supported in part by grants from the National Science Foundation and Office of Naval Research.

■ REFERENCES

(1) (a) Tsuda, T.; Hussey, C. L. *Electrochem. Soc. Interface* **2007**, *16*, 42–49. (b) Forsyth, S. A.; Pringle, J. M.; MacFarlane, D. R. *Australia J. Chem.* **2004**, *57*, 113–119.

(2) Lopes, J. N. C.; Gomes, M. F. C.; Padua, A. A. H. *J. Phys. Chem. B* **2006**, *110*, 16816–16818.

(3) Canongia Lopes, J. N.; Padua, A. A. H. *J. Phys. Chem. B* **2006**, *110*, 19586–19592.

(4) Silvester, D. S.; Aldous, L.; Hardacre, C.; Compton, R. G. *J. Phys. Chem. B* **2007**, *111*, 5000–5007.

(5) Ye, C.; Shreeve, J. M. *J. Phys. Chem. A* **2007**, *111*, 1456–1461.

(6) Lynden-Bell, R. M. *J. Phys. Chem. B* **2007**, *111*, 10800–10806.

(7) Rickert, P. G.; Antonio, M. R.; Firestone, M. A.; Kubatko, K.-A.; Szreder, T.; Wishart, J. F.; Dietz, M. L. *J. Phys. Chem. B* **2007**, *111*, 4685–4692.

(8) (a) Kulesza, P. J.; Dickinson, E.; Williams, M. E.; Hendrickson, S.; Murray, R. W. *J. Phys. Chem. B* **2001**, *105*, 5833–5838. (b) Dickinson, E.; Masui, H.; Williams, M. E.; Murray, R. W. *J. Phys. Chem.* **1999**, *103*, 11028–11035.

(9) Harper, A. S.; Lee, D.; Crooker, J. C.; Wang, W.; Williams, M. E.; Murray, R. W. *J. Phys. Chem. B* **2004**, *108*, 1866–1873.

(10) Harper, A. S.; Leone, A. M.; Lee, D.; Wang, W.; Ranganathan, S.; Williams, M. E.; Murray, R. W. *J. Phys. Chem. B* **2005**, *109*, 18852–18859.

(11) (a) Leone, A. M.; Brennaman, M. K.; Tibodeau, J. D.; Papanikolas, J. M.; Murray, R. W.; Thorp, H. H. *J. Phys. Chem. B* **2003**, *107*, 6469–6473.

(b) Leone, A. M.; Hull, D. O.; Wang, W.; Thorp, H. H.; Murray, R. W. *J. Phys. Chem. A* **2004**, *108*, 9787–9793. (c) Leone, A. M.; Tibodeau, J. D.; Bull, S. H.; Feldberg, S. W.; Thorp, H. H.; Murray, R. W. *J. Am. Chem. Soc.* **2003**, *125*, 6784–6790.

(12) Williams, M. E.; Lyons, L. J.; Long, J. W.; Murray, R. W. *J. Phys. Chem.* **1997**, *101*, 7584–7591.

(13) (a) Lee, D.; Hutchison, J. C.; Leone, A. M.; DeSimone, J. M.; Murray, R. W. *J. Am. Chem. Soc.* **2002**, *124*, 9310–9317. (b) Leone, A. M.; Weatherly, S. C.; Williams, M. E.; Thorp, H. H.; Murray, R. W. *J. Am. Chem. Soc.* **2001**, *123*, 218–222.

(14) Wang, W.; Balasubramanian, R.; Murray, R. W. *J. Phys. Chem. C* **2008**, *112*, 18207–18216.

(15) (a) Ranganathan, S.; Murray, R. W. *J. Phys. Chem. B* **2004**, *108*, 19982–19989. (b) Williams, M. E.; Lyons, L. J.; Long, J. W.; Murray, R. M. *J. Phys. Chem. B* **1997**, *101*, 7584.

(16) Wang, W.; Lee, D.; Leone, A. M.; Murray, R. W. *Chem. Phys.* **2005**, *319*, 126–135.

(17) Lee, D.; Harper, A. S.; DeSimone, J. M.; Murray, R. W. *J. Am. Chem. Soc.* **2003**, *125*, 1096–1103.

(18) Buttry, D. A.; Anson, F. C. *J. Electroanal. Chem.* **1981**, *130*, 333–338.

(19) (a) Dahms, H. *J. Phys. Chem.* **1968**, *72*, 362. (b) Ruff, I.; Friedrich, V. J. *J. Phys. Chem.* **1971**, *75*, 3297.

(20) Majda, M. In *Molecular Design of Electrode Surfaces*; Murray, R. W., Ed.; John Wiley & Sons: New York, 1992.

(21) Marcus, R. A. *J. Phys. Chem. B* **1998**, *102*, 10071–10077.

(22) Carbonell, E.; Andres, J. L.; Lledos, A.; Duran, M.; Bertran, J. *J. Am. Chem. Soc.* **1988**, *110*, 996–1001.

(23) Chen, H.; Kwait, D. C.; Goenen, Z. S.; Weslowski, B. T.; Abdallah, D. J.; Weiss, R. G. *Chem. Mater.* **2002**, *14*, 4063–4072.

(24) Vogel, M.; Rausch, M.; Rosenberg, H. *J. Org. Chem.* **2002**, *22*, 1016–1018.

(25) (a) Bard, A. J.; Faulkner, L. R. *Electrochemical Methods: Fundamentals and Applications*, 2nd ed.; Wiley and Sons: New York, 2001. (b) The current versus time$^{-1/2}$ Cottrell plot is according to the equation $i = nFAD^{1/2}C_{Fc}/\pi^{1/2}t^{1/2}$.

(26) (a) Marcus, R. A.; Sutin, N. *Biochim. Biophys. Acta* **1985**, *811*, 265.(b) Marcus, R. A.; Siddarth, P. In *Photoprocesses in Transition Metal Complexes, Biosystems, and Other Molecules*; Kochanski, E., Ed.; Kluwer Academic Publishers: Dordrecht, The Netherlands, 1992.

(27) Andrieux, C. P.; Saveant, J. M. *J. Phys. Chem.* **1988**, *92*, 6761–6767.